PHYSICAL REVIEW A VOLUME 24, NUMBER 5 NOVEMBER 1981

Observation of harmonics in the visible and ultraviolet created in CO_2-laser-produced plasmas

R. L. Carman, C. K. Rhodes,* and R. F. Benjamin
Los Alamos National Laboratory, Los Alamos, New Mexico 87545
(Received 22 May 1981)

Experimental studies of inertially confined plasmas irradiated with CO_2 laser intensities greater than 10^{15} W/cm^2 at 10.6-μm wavelength reveal the generation of harmonic spectral components up to the 46th order ($\sim$230 nm). These harmonics are of very short duration ($<$200 ps), have a polarization parallel to that of the incident 10.6-μm electric field, and exhibit a conversion efficiency approximately independent of the harmonic order up to a maximum order. The plasma-physics phenomena responsible for the high-harmonic emission are examined. The data and theory are consistent with the presence of self-focusing.

I. INTRODUCTION

The generation of laser harmonics in dense, laser-produced, high-temperature plasmas has been under study for years.[1-6] Many properties of these harmonic spectra produced by irradiation at both 1 and 10 μm on solid targets have been reported, mostly for the three-halves, second, and third harmonics. Until recently the highest harmonic light observed in CO_2 laser target interaction experiments was the 11th seen by Burnett *et al.*[4] In more classical nonlinear-optics experiments the ninth harmonic has been produced directly in metal vapors,[7] and the seventh harmonic of a quadrupled Nd:YAG laser ($\sim$38 nm) was observed in rare gases.[8]

Recently, at least 28 harmonics have been seen[6] in CO_2-laser-produced-plasma experiments in which the nonlinear response was strongly affected by density-profile modifications of the laser-induced plasma. Numerical simulation of the nonlinear response at high intensity is severely step-size limited; thus, the precise relationship between observed harmonic spectra and density profile is understood only at lower intensities. For high intensities and longer wavelengths [I (W/cm^2) $\times\lambda^2$ (μm)$>10^{16}$] plasma-density profiles are known to be appreciably modified by radiation pressure.[5,6,9] Laser interferometry has directly verified these steepened density profiles,[10] but only recently[6] was a density jump from $N\sim 0.1\ N_{\text{critical}}$ $\sim 10^{18}\ e/\text{cm}^3$ to $N>400\ N_{\text{critical}}$ $\sim 4\times 10^{21}\ e/\text{cm}^3$ in a spatial distance $<<0.1\ \lambda\sim 1\ \mu$m inferred for the first time. In the presence of a density jump, a longitudinal Langmuir wave is created along the plasma surface and the high nonlinearity of this wave is believed to be responsible for the production of the high harmonics observed.

We report the first observation of spectra exhibiting at least the 46th harmonic ($\sim$230 nm) of 10.6-μm incident radiation. The intensity of the harmonic spectra lines was nearly constant from $\sim$662 to $\sim$252 nm (16th to 42nd harmonics). Harmonics below the 16th order were not observed because only visible- and ultraviolet-light-sensitive films were used. We did not search for harmonics at wavelengths below 252 nm because the detection system had not yet been calibrated for this range.

High-order half-integral spectra up to the $\frac{87}{2}$ harmonic were also observed. Although conversion efficiencies for the half-integral harmonics varied appreciably and were always lower than those for the integral harmonics, the intensities of these two groups were occasionally within one order of magnitude of each other.

The principal experimental results of our studies are presented in Sec. II including the spectral and temporal characteristics of the harmonic radiation, the degree of polarization, and the efficiency of conversion associated with the production of harmonics. While previous models for numerical calculations of the harmonic spectra observed at low and intermediate intensities were satisfactory,[6] our findings suggest the need for a simple model that would account for the basic characteristics of the observed harmonic generation in the limiting case of high incident laser intensity. A lower bound to this model is described in Sec. III. If this lower

bound is to agree with our data a mechanism for increasing the laser intensity must be considered. The possibility of self-focusing is discussed in Sec. IV. In light of the extreme nonlinear response associated with the production of more than 40 harmonics at an efficiency of $\sim 10^{-4}$ to 10^{-5} such evaluation appears to be warranted. Finally, Sec. V summarizes the conclusions of our studies.

II. EXPERIMENTAL RESULTS

Our experiments were conducted with one of the beams at the Los Alamos Gemini laser facility. The incident laser energy could be varied from 100 to 300 J while the laser pulse duration was kept about constant at 1–2 ns FWHM (full width at half maximum). The oscillator was operated on only one line, namely, the $P20$ transition in the 10-μm band. The targets were 25-mm long and either solid cylindrical carbon wires nominally 250 μm in diameter or 1-μm CH-overcoated BeCu wires, again nominally 250 μm in diameter. The laser was focused by an $f/2.4$ off-axis parabolic mirror to the center of the wire. Laser intensities on target were determined from their phenomenologically established correlation with maximum proton velocities.[11]

Most of the spectra were obtained with a 0.5-m Model-216.5 vacuum McPherson spectrograph which was fastened directly to the Gemini target chamber. The scattered harmonic light was collected by an aluminum spherical mirror with a radius of curvature of 25 cm ($f/3$ effective) and relayed to the entrance slit of the spectrograph at $\sim 7\times$ magnification. This arrangement precluded high spatial resolution (limited to ~ 15-line pairs/mm) due to the aberrations but greatly increased the solid angle subtended by the slits. Two different gratings were used, both in first order. One was a 600-lines/mm grating blazed at 500 nm whereas the second was a 1200-lines/mm grating blazed at 150 nm. Two different films, namely, Kodak type-2485 instrumentation film and Kodak 103 type-O scientific film, were used with and without uv sensitizer coatings. Furthermore, the type-2485 film was processed in Kodak 857 developer at 90 F to maximize the sensitivity and the usable dynamic range.

A second 1.0-m Model-216 McPherson spectrograph monitored the visible harmonics from 700 to 400 nm, while the 0.5-m spectrograph was stepped through the spectral region from 690 to 230 nm. The transmission relay lenses of ~ 250-mm focal length ($\sim f/5$) had been used in previous work.[6] A 300-lines/mm grating blazed at 1 μm was used in second order with Kodak 2485 instrumentation film, which was also processed in 857 developer.

The direction of observation for both spectrographs was in the horizontal plane containing the axis of the incident laser focusing parabola, as shown in Fig. 1. The 0.5-m spectrograph was located at $\sim 105°$ around from the laser optic axis in

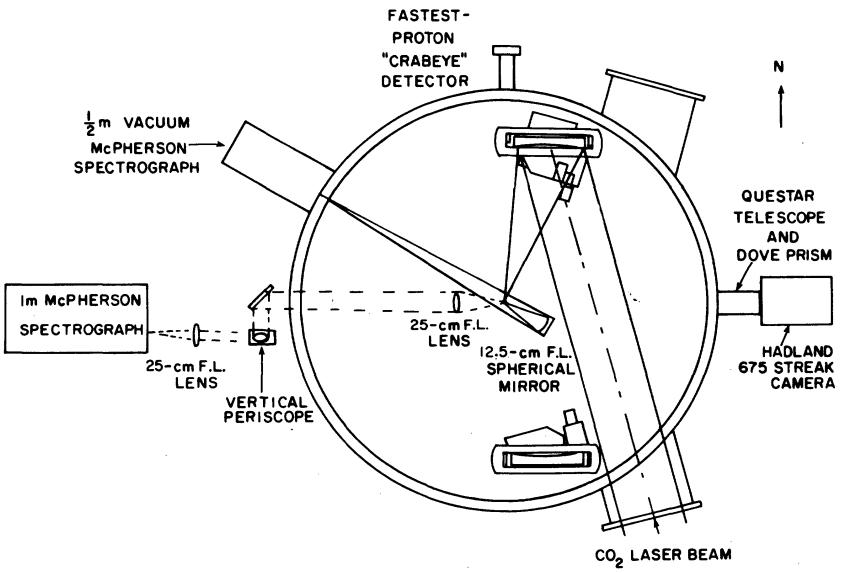

FIG. 1. Top view of the Gemini target chamber indicates the approximate locations of key diagnostics and of the laser beam. Particle detectors and x-ray diagnostics were also present.

one direction, whereas the 1-m instrument was $\sim 105°$ around from the laser optic axis in the opposite direction. Both were aligned by demanding that a HeNe laser beam, focused on the output plane of either spectrograph, retrace the optical-collector path and focus on the target surface within the CO_2 focal area.

A Hadland Model-675 fast visible-light streak camera was located directly opposite the 1-m spectrograph. The camera was used to study the temporal properties of the harmonic light. The target imaging system consisted of a Questar telescope and a dove prism which made it possible to change the orientation of the slit of the streak camera relative to the target axis.

Microdensitometer traces of spectra obtained at an incident intensity of $\sim 2\times 10^{15}$ W/cm^2 are shown in Fig. 2. As noted above, the intensity is inferred from the velocity of the fastest protons emitted by the front of the target.[11] Actually, three lasers shots were required to cover the entire spectrum from the 17th through the 46th harmonic. These spectra were obtained with the 0.5-m spectrograph, the 600-lines/mm grating, and instrumentation film that was processed as previously described.

An ultraviolet continuum, beginning at ~ 480 nm and continuing into the short-wavelength region, is apparent. The film we used had been coated with a Kodak A3177 sensitizer to enhance the uv sensitivity. However, when combined with the processing used, the spectral sensitivity for wavelengths shorter than 300 nm varied greatly. By switching to Kodak 103 type-O plates and over-

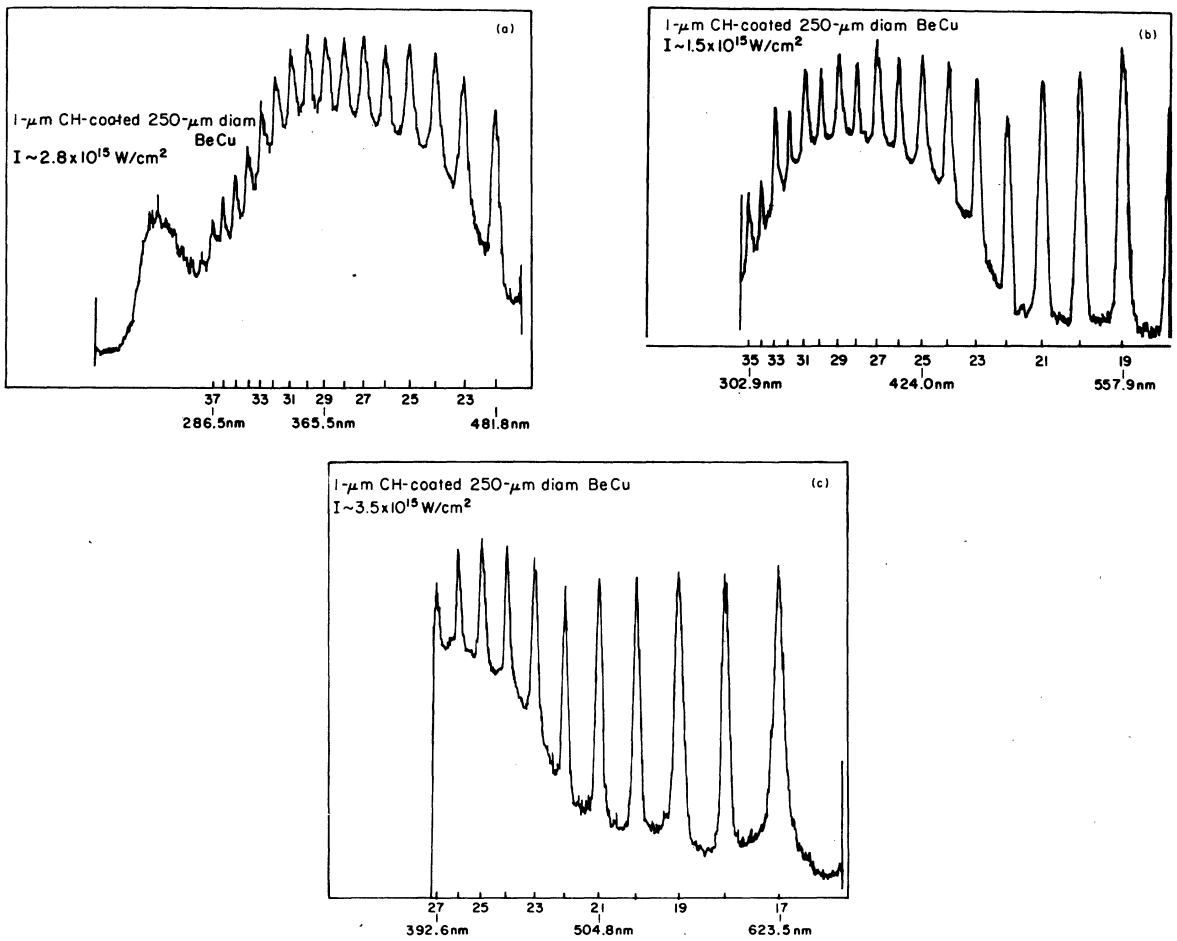

FIG. 2. Microdensitometer traces of the raw data taken with the 0.5-m vacuum spectrograph, 600-lines/mm grating blazed at 500 nm, and Kodak 2485 film. The numbers on the abscissa indicate the harmonic order of the $P20$ transition in the 10-μm band. Three different shots are shown with the intensities on target indicated where the center wavelength of the spectra was shifted between shots.

coating the plates with Kodak A3177 uv sensitizer, we obtained a system that was more amenable to accurate calibration, but was less sensitive. A spectrum, obtained with such plates at essentially the same laser intensity, but with the 1200-lines/mm grating blazed at 150 nm, is shown in Fig. 3.

The spectrum at wavelengths shorter than the 42nd harmonic (~252 nm) was inaccurate due to contamination of the vacuum chamber. The vacuum in both spectrograph and chamber was $>3\times10^{-5}$ Torr due to large quantities of plastic in the target chamber. Since the absorption over the 4-m optical path appears to have altered the spectrum we have disregarded these data.

In contrast, Fig. 4 illustrates a microdensitometer scan of a similar spectrum taken under the same conditions as that shown in Fig. 2, except that the laser intensity was lowered to 10^{14} W/cm^2. Note the rapid falloff in the energy conversion of the harmonic light for orders above 20. This spectrum is more typical of the Gemini spectra discussed in our previous report.[6]

The relative conversion efficiencies for the visible harmonics of the spectra shown in Figs. 2–4 were the same to within an uncertainty of ~50% from the 16th through the 42nd harmonic after the proper correction factors had been applied to the direct microdensitometer traces shown. To determine these correction factors we performed a spectral radiometric calibration of the instrument as well as studies of the saturation properties as a function of frequency of both the 2485 and 103 type-O films. Because of the large number of factors involved, it does not appear practical to attempt to appreciably reduce this uncertainty.

Because the solid angle of observation for the harmonic radiation was relatively small, the angu-

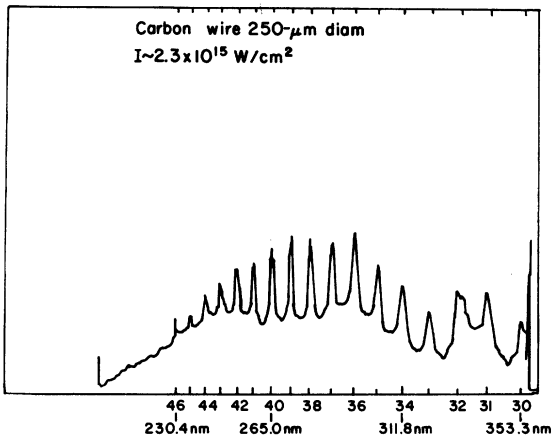

FIG. 3. Microddensitometer trace of the raw data taken with the 0.5-m vacuum spectrograph, 1200-lines/mm grating blazed at 150 nm, and Kodak 103 type-O film which had been uv sensitized.

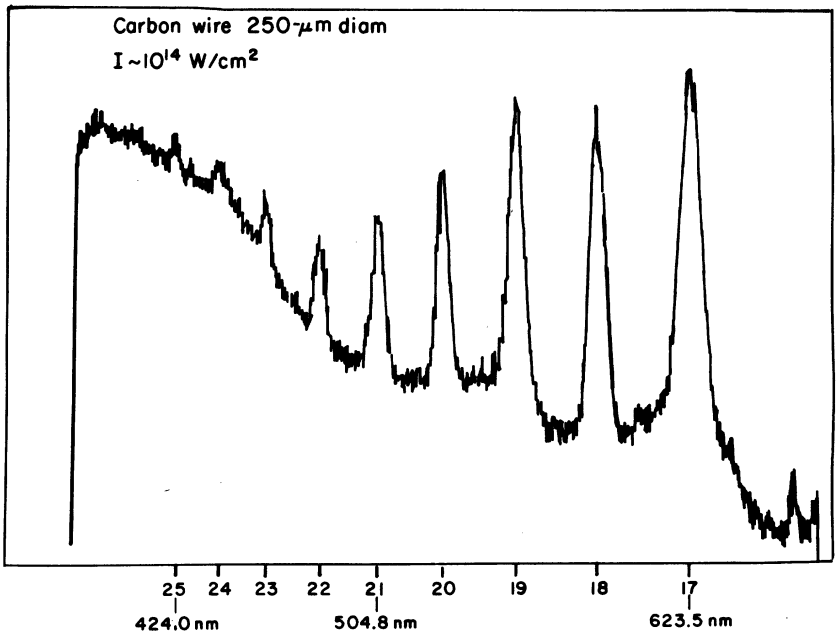

FIG. 4. Microdensitometer trace of the spectrum taken with the 0.5-m vacuum spectrograph, 600-lines/mm grating blazed at 500 nm, and Kodak 2485 film showing an example similar to the spectra shown in Fig. 6 for lower laser intensities.

lar distribution of harmonic intensity was not established. Therefore, in estimating the efficiency of harmonic production, an isotropic distribution was assumed, a choice motivated by the previous studies of Lee *et al.*[2] This assumption yields an efficiency of $\sim 10^{-4}-10^{-5}$ per order, a value affirming the previous estimate[6] for conversion of incident CO_2 light to high-order harmonics.

Odd-integer and even-integer harmonics do not always have the same conversion efficiency. Microdensitometer traces of two such spectra taken on consecutive shots under nearly identical conditions are shown in Fig. 5. Note the significantly higher conversion into even harmonics (by a factor of 2 when fully analyzed). Conversely, Fig. 6 illustrates a counterexample in which the odd harmonics dominated, although fewer total harmonics were generated. Note that for both Figs. 5 and 6 the incident laser intensities inferred from the velocity of the fastest proton were essentially the same, a point that will be discussed more fully in the following sections.

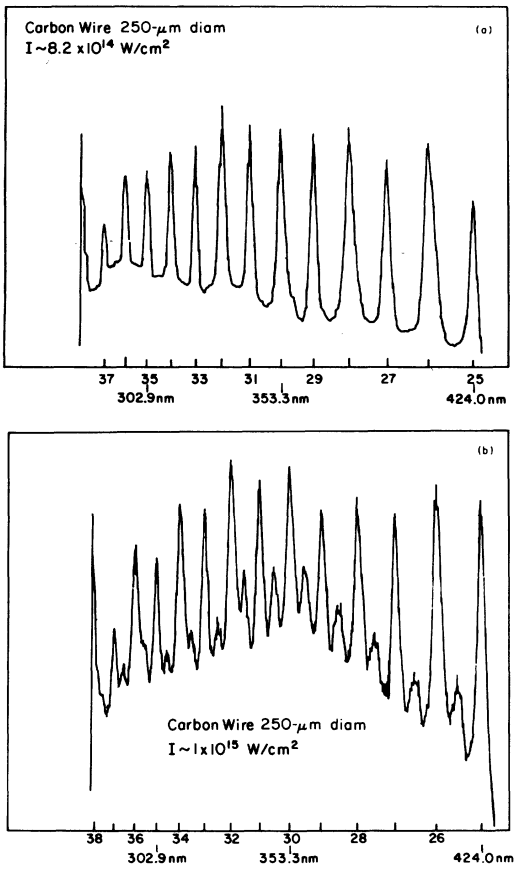

FIG. 5. Microdensitometer traces of the raw data taken with the 0.5-m vacuum spectrograph, 600-lines/mm grating blazed at 500 nm, and Kodak 2485 film shown for sequential shots under nearly identical conditions. The top spectrum shows a small variation in odd-to-even harmonic production efficiency and no half-integer harmonics. The bottom spectrum shows an accentuation of the alternation in harmonic efficiency where more even-harmonic light is produced than odd and the presence of half-integer harmonics is clear.

The spectra of both Fig. 5 (bottom) and Fig. 6 show the presence of half-integer harmonic light. In both cases the half-integer harmonics appear to be ~ 30 times less intense and do not extend over the full spectral range of the integer-harmonic spectrum. Half-integer harmonics are a prominent feature of many spectra, as shown in Fig. 7. Spectra containing these frequencies were always observed in conjunction with significant changes in the ion blowoff distributions, a fact implying appreciable changes in target alignment. Note that considerable harmonic power is contained in the half-integer harmonic components; the 32nd and $\frac{65}{2}$, for example, differ only by a factor of 5 in radiated energy for the spectrum shown in Fig. 7.

The polarization of the harmonic light has been studied by using both spectrographs simultaneously in the region extending from 400 nm (26th harmonic) through 700 nm (16th harmonic). In this measurement, the 0.5-m vacuum spectrograph was used to monitor the harmonic yield whereas a Polaroid sheet polarizer was placed in the light path to the 1-m spectrograph. With this technique the harmonic light in the visible range was more than 90% polarized along the polarization direction of the incident 10-μm radiation (normal to the plane of Fig. 1). Note that the laser light is *s* polarized for the initial target surface. Of course, radiation-pressure-induced craters and surface ripples in the density profile can convert the *s* into *p* polarization.

Spatially resolved, time-integrated harmonic photographs of the CO_2 laser focal area have been taken at the eight-beam Helios laser facility with a 4×5 in.^{2} Graflex camera, a Questar telescope (1000-mm equivalent focal length), and Kodak 2485 film with hot processing. This new diagnostic appears to allow accurate location of the focal centers, their relative positions, and their approximate diameters. By defocusing the laser beam, the spot-size variation was found to track the previously measured spot size for 80% of the incident laser energy. With the insertion of band-pass filters of <10-Å width centered on the 16th and 20th harmonics of the *P*20 10-μm wavelength, no change

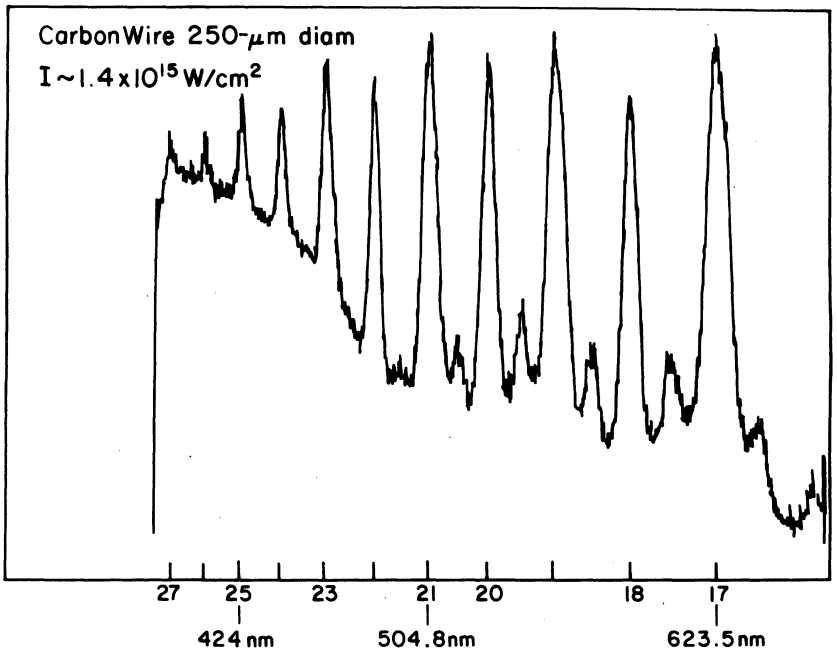

FIG. 6. In contrast to the spectrum of Fig. 5 we note that for a similar incident intensity the alternation in harmonic production efficiency is still present, but more odd-harmonic light is produced than even.

in the visible intensity pattern was detected in comparison to that simultaneously observed without the use of any spectral filtering.

To establish the temporal characteristics of the harmonic radiation, the Hadland Model-675 streak camera was mounted on the Gemini target chamber in the position indicated in Fig. 1. No spectral filtering was used. Figure 8 shows a mi-

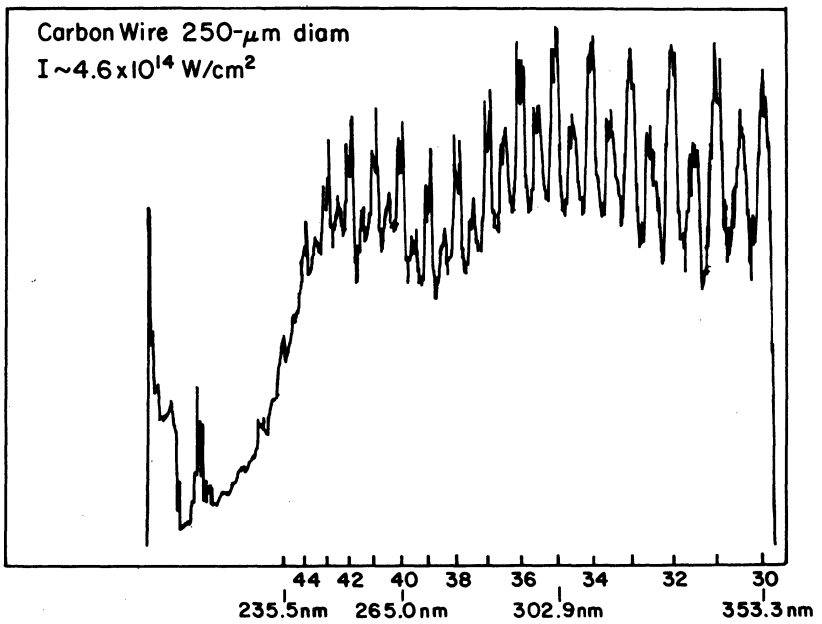

FIG. 7. Microdensitometer trace of the raw data taken with the 0.5-m vacuum spectrograph, 600-lines/mm grating blazed at 500 nm, and Kodak 2485 film coated with uv sensitizer. Note the large quantity of half-integer harmonic light as well as the presence of fine structure. The $\frac{65}{2}$ harmonic has 20% of the light contained in the 32nd harmonic.

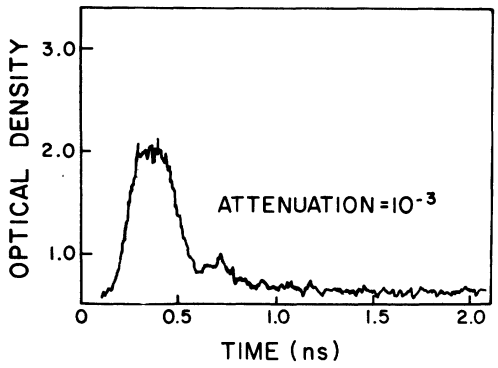

FIG. 8. Microdensitometer trace of a streak-camera record of the visible light emitted from the carbon-wire target. The early bright region is believed to be associated with the harmonic light and is <200 ps in duration. The remaining light is associated with the plasma expansion. The sweep speed is 0.4 ns/mm and time increases to the right. A reduction in attenuation of 100-fold leads to a fully saturated trace of optical density 3.0.

crodensitometer trace of a streak record taken at neutral density (ND) 3.0 attenuation. Note the bright, small dot followed by a weaker, expanding light region. The light intensity in the small spot is >100 times higher than the intensity in the less luminous expanding region. The initial bright spot, which lasted <200 ps, is interpreted as the harmonic radiation. Because no other radiation is detected prior to that attributed to the harmonics, we conclude that the harmonic light is generated only in the initial rising portion of the CO_2 laser pulse. This interpretation is fully consistent with the work at Helios and the work of Caruso *et al.*[2] but differs from that of Richardson.[12] The fact that the harmonic light is generated only over such a short-time interval implies that the harmonic conversion efficiencies quoted earlier relate only to energy conversion. The intensity conversion efficiencies could be appreciably higher.

III. THEORETICAL ANALYSIS

We wish to use the extraordinary features of these spectra to improve our understanding about the plasma conditions and the laser-plasma interaction. Although an exact calculation, analytical or numerical, is beyond current understanding of these complex processes we can identify the necessary components of such a calculation. Our analysis will proceed in three steps of increasing complexity. First, we describe the fundamental form of the electron force function that generates the harmonics. This analysis is based on Fourier analysis of the spectra. Then we estimate the conversion efficiency from 10.6-μm light into high harmonics by using a simple model of radiation from noninteracting electrons that are accelerated by the electric field of the 10.6-μm illumination. This heuristic model underestimates the conversion efficiency as expected. Lastly, we turn to plasma simulation and analyze a key result, that is, the scaling law for the highest harmonic produced. The inadequacies of these models, single-particle electrodynamics and plasma simulation, suggest additional plasma processes, collective effects, and enhanced laser intensity. We explore enhanced laser intensity in detail in the form of self-focusing in Sec. IV.

Some general characteristics of the force function that generates the harmonics are apparent from a simple Fourier analysis of the spectra. The spectral width implies either an exceedingly fast rise-time, or falltime, or temporal structure of the emitter. The bandwidth $\Delta\nu=4\times10^4$ cm^{-1} for 46 harmonics corresponds to a time constant ~0.3 fs. Thus, harmonic generation occurs during a very short fraction of an optical cycle of the 10.6-μm fundamental wavelength. This temporal structure constitutes a major obstacle to numerical calculations attempting to model the interaction. An accurate simulation requires step sizes smaller than the time constant of 0.3 fs in order to obtain the necessary temporal resolution. Such a resolution is far beyond the practical capabilities of current simulations.

The periodic structure of the harmonic spectrum implies a temporal periodicity in the force function. A heuristic model for such behavior is an extremely steep density profile in which the fundamental is mixed with the nth harmonic to produce the $(n+1)$th harmonic, up to the highest harmonic.[6] A mechanism for producing such a steep profile is radiation pressure. This model of mixing predicts that the highest harmonic simply corresponds to the wavelength for which its critical density is the plasma density of the upper shelf. Thus the highest harmonic is believed to give information on the density at the profile's upper shelf.

Another noteworthy feature of the spectra is the lack of variation of spectral intensity with the order of the harmonic. These results differ from measurements taken elsewhere[4] at lower irradiance, plotted in Fig. 9. Our results suggest that the emission mechanism is "saturated" above $I\lambda^2>10^{17}$ Wμm^2/cm^2 and that a perturbation theory is not applicable. Furthermore, the square

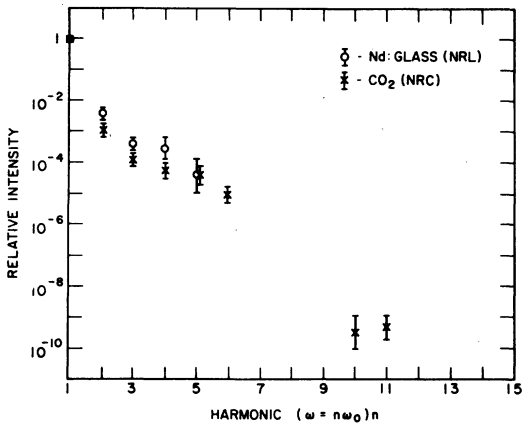

FIG. 9. Replot of the data presented in Ref. 4 of the observed conversion efficiency of harmonic light normalized to the fundamental laser backscattered light for several harmonic orders. Note the nearly linear falloff of the conversion efficiency with harmonic order. These data were taken for I (W/cm^2) λ^2 (μm)$\sim 10^{16}$.

envelope of the spectrum implies that the time dependence of the force approaches that of a periodic array of delta functions. Thus the force is highly impulsive. We use this inference about the impulsive nature of the force to approximate a single-particle calculation.

A simple single-electron representation can be used to estimate the intensity of the harmonic radiation. This is done, with the neglect of $\vec{v}\times\vec{B}$ forces in a manner similar to that used by Kaw and Dawson,[13] by considering a particle of charge e and mass m subjected to the electric force

$$\vec{F}=e\vec{E}\,, \tag{1}$$

in which E represents the optical-field strength. With this simple force function, the particle acceleration and thus the radiation rate can be computed from standard classical arguments. Such a single-particle description of course is incorrect because it underestimates the radiated harmonic power by ignoring collective motions. It is of interest therefore to compare the harmonic conversion derived in this simple way to that actually observed and thus to obtain a direct indication of the role of collective motions.

With this approach the Larmor formula can be used to find the power radiated[14] into the highest harmonic $n_{\max}$ from

$$P_{n_{\max}}=\frac{2}{3}\frac{e^2}{c^3}|\vec{a}|^2\,, \tag{2}$$

in which $|\vec{a}|$ is the magnitude of the particle acceleration. This gives the result

$$P_{n_{\max}}=\frac{\alpha}{6\pi^2}\hbar n_{\max}^2\omega^2\,, \tag{3}$$

in which $\omega=2\pi/T$ is the angular frequency of the fundamental and $\alpha=e^2/\hbar c$. Equation (3) breaks naturally into three factors; one involving α which represents the basic coupling strength, an energy scale factor $\hbar n\omega$ representing the magnitude of the quantum, and a characteristic inverse time $n\omega$. Applied in the high-intensity limit $eE\lambda/m_0c^2\simeq 1$, this result applies for incident laser intensities I_n (in W/cm^2) given by

$$I_n=\left[\frac{n^2c}{8\pi\alpha}\right]\left[\frac{m_0c^2}{\lambda\!\!\!^{-}_c\lambda^2}\right]\,, \tag{4}$$

in which $\lambda\!\!\!^{-}_c$ is the electron Compton wavelength and λ is the fundamental wavelength. While relativistic corrections could have been included in Eqs. (2)—(4), they do not drastically alter these results.

For the stated conditions we can now evaluate the ratio $\eta_{n_{\max}}$ of the intensity scattered in the maximum harmonic to the intensity of illumination of the fundamental. This parameter therefore represents the efficiency of maximum-order harmonic production. The intensity scattered in the harmonic wave $I_H(n)$ is given by

$$I_H(n)=P_n\rho_e\delta\,, \tag{5}$$

in which ρ_e is the local electron density and δ is the penetration skin depth of the fundamental radiation for density ρ_e. From the results of Kaw and Dawson[13] the skin depth δ is given by

$$\delta=\frac{e}{i\omega\epsilon^{1/2}}\Big|_{\rho_e}\sim(4\pi\rho_e\lambda\!\!\!^{-}_c\alpha)^{-1/2}\,, \tag{6}$$

in which

$$\epsilon=1-\frac{\omega_P^2}{\omega^2}\left[1+\frac{e^2E^2}{m^2c^2\omega^2}\right]^{-1/2}\,. \tag{7}$$

To evaluate the local electron density ρ_e it is necessary to estimate the discontinuity in plasma density near the critical surface associated with the plasma profile modification arising from the radiation pressure. We assume that all harmonic waves have a maximum spatial overlap with the fundamental. This situation is obtained provided that the critical density N_{critical} for all the n harmonics are spatially collocated.[6] [Note that the critical densities $N_{\text{critical}}(\omega)$ are defined as the electron density at which the plasma dielectric constant goes to zero for the fundamental light frequency ω.] Phys-

ically this condition requires the existence of a discontuinity in plasma density. As noted previously[9,10] radiation causes the spatial profile of the electron density to be modified inducing a sharp gradient in density. The necessary conditions are satisfied if the effective upper density N_{upper} is such that

$$N_{\text{upper}} \cong n_{\text{max}}^2 N_{\text{critical}}(\omega) , \tag{8}$$

in which n_{max} is the order of the maximum harmonic observed. This relationship has been found to be a good approximation in previous studies.[6] It implies that the inverse of the skin depth δ^{-1} vanishes for the frequency of the highest harmonic, $n_{\text{max}}\omega$. Therefore, we set $\rho_e = N_{\text{upper}} = n_{\text{max}}^2 N_{\text{critical}}(\omega)$ in which

$$N_{\text{critical}}(\omega) = \frac{4\pi e^2}{m_0 \omega^2} = \frac{\pi}{\alpha \lambda\!\!\!^{-}_c \lambda^2} . \tag{9}$$

Substitution of the above expressions into Eq. (5) now yields

$$I_H(n_{\text{max}}) = \frac{P_{n_{\text{max}}} n_{\text{max}}^2}{2\alpha \lambda\!\!\!^{-}_c \lambda} , \tag{10}$$

the magnitude of the power scattered into highest-order harmonics. From Eqs. (3), (4), and (10) it is now possible to estimate the efficiency of the maximum harmonic as

$$\eta_{n_{\text{max}}} = \frac{16\pi^5}{3} \alpha^2 \lambda\!\!\!^{-2}_c \rho_e \delta = \frac{8\pi^5}{3} \alpha \lambda\!\!\!^{-}_c \frac{n_{\text{max}}}{\lambda} = \frac{2.5 \times 10^{-8}}{\lambda_{n_{\text{max}}}(\mu\text{m})} , \tag{11}$$

in which $\lambda_{n_{\text{max}}}$ is the wavelength of the maximum harmonic produced. For Fig. 3, where $\lambda_{n_{\text{max}}} = 10.6\ \mu\text{m}/42 = 0.25\ \mu\text{m}$ we find $\eta_{n_{\text{max}}} = 1 \times 10^{-7}$, whereas $I_{n_{\text{max}}} \sim 5.5 \times 10^{17}$ W/cm^2 from Eq. (4).

In the above discussion we identified a lower bound on the efficiency of producing the maximum observed harmonics but did not evaluate the harmonic spectral distribution. Although even harmonics are copiously generated experimentally, these components in homogeneous isotropic media, due to symmetry, have zero amplitude. The role of the plasma surface for even-harmonic production[2] is therefore implied. Transition radiation arising from a uniformly moving charge crossing a boundary between two media is to be expected[15] but has been neglected. It is the transition radiation in the single-particle model, which is called Langmuir waves within a collective many-body treatment, that was identified as being responsible for the production of the harmonics in previous work.[6] Also, a plasma with a large jump in density within a small region of space shares some nonlinearities with a metallic boundary,[16] which have also been neglected. The discussion above of course only applies to a homogeneous bulk medium containing noninteracting electrons. From considerations of these factors it should not be surprising that different conversion efficiencies exist for odd and for even harmonics. It is therefore unexpected to find that the conversion efficiencies for both odd and even harmonics are comparable for many of our spectra.

The discrepancies between our data and a simple model based on single-particle electrodynamics motivate the need for a more detailed calculation. Such a calculation involving a plasma simulation is presented in Ref. 6 but this work estimated harmonic production only up to the eighth, which is far less than the number of harmonics we observed. However, an important, useful result of this simulation is the scaling of n_{max} with laser intensity I and cold-electron temperature T_c. This scaling law is compared with data below and provides further support for the existence of self-focusing.

For conditions leading to the production of the eighth harmonic, the numerical model of Ref. 6 found that the number n_{max} of the highest harmonic produced is expected to scale like

$$n_{\text{max}} \propto (I\lambda^2/T_c)^{1/2} . \tag{12}$$

Because our experiments have been performed at a fixed wavelength, and recalling that the results shown in Fig. 9 confirm that a constant $I\lambda^2$ generates a similar harmonic spectrum, we have plotted n_{max} versus incident laser intensity I as inferred from the highest proton velocity measured (Fig. 10). The straight lines in the plot correspond to lines of slope $\frac{1}{2}$ depicting the expected square-root dependence of n_{max} on I. In the lower left-hand corner we have included a data point taken from Fig. 9 for which $I \sim 10^{14}$ W/cm^2. A break in the linear falloff of harmonic efficiency in Fig. 9 is suggested at $n \sim 4$.

To assign a temperature to each line on Fig. 10 we estimate the radiation pressure

$$P_L = \frac{E^2}{8\pi}(2-A) = \frac{I}{c}(2-A) , \tag{13}$$

where A is the absorbed fraction. We assume that only absorption and reflection occur. Although this expression does not deal correctly with the

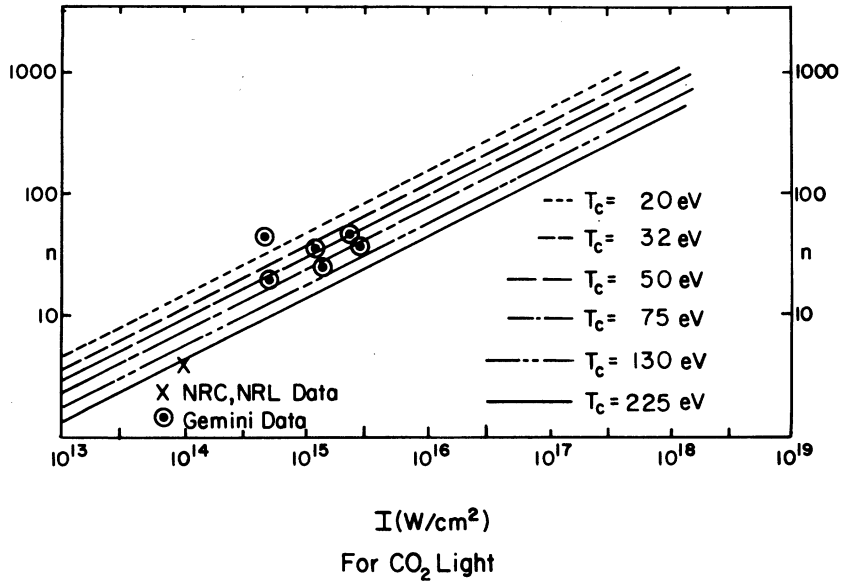

FIG. 10. Plot of the maximum number of harmonics produced efficiently vs incident CO_2 laser intensity as inferred from fastest-proton velocity. The data from Fig. 9 are included although there is some uncertainty regarding the proper relative intensity. The cold-plasma temperature assigned to each theoretical line of slope $\frac{1}{2}$ is obtained from the pressure balance.

light that is refracted or enhanced due to dielectric field enhancement where ϵ approaches 0, we assume that the fraction of light involved in these processes is sufficiently small to be neglected. Now the hydrodynamic expansion pressure P_p is obtained from an ideal-gas approximation, namely,

$$P_p = NkT = N_{\text{upper}} T_c \ , \tag{14}$$

in which T_c is the temperature (eV) of the cold background plasma. Equation (14) assumes a fully ionized plasma. We set Eqs. (13) and (14) equal to each other and solve for T_c, using Eqs. (8) and (9), thereby leading to

$$T_c = (2-A)\frac{I\lambda^2}{n_{\max}^2}\left[\frac{\alpha\lambda_c}{\pi c}\right] . \tag{15}$$

Separate measurements aimed at determining the absorbed fraction suggest[17] that $A \simeq 0.3$. These results have been used to obtain the values of T_c noted parametrically on Fig. 10. Most of the data lie between $T_c = 50$ eV and $T_c = 130$ eV, which is somewhat colder than the usual estimates based on x-ray spectra. However, if the harmonic light is produced only during the early, rising portion of the CO_2 laser pulse, then lower temperatures are expected; peak x-ray signals which lead to higher T_c estimates are calculated and observed to occur at the peak of the laser pulse. Note that one data point is consistent with $T_c \sim 5$ eV. We shall return to this point later in Sec. IV.

We now briefly turn to the half-integer harmonic spectra. We note that some natural selection of the half-integer harmonic exists because

$$(n+\tfrac{1}{2})\omega_L = [(n+1)-\tfrac{1}{2}]\omega_L \ . \tag{16}$$

Thus a particular half-harmonic component can be produced by parametrically beating with the integer harmonic on either side. Note that the high-integer harmonics can also be generated parametrically. Thus a more complete treatment of high-harmonic generation will have to take these parametric processes into account. On the other hand, the presence of high half-integral harmonic light very likely implies that half-harmonic light, presumably from stimulated Raman scattering, is also present.

Although the simple description given above is not a full analysis of the plasma response, it indicates the key features that must be incorporated. The impulsive nature of the force function appears unavoidable, a fact evident directly from recorded spectra. The radiation-pressure effects and the concomitant plasma-profile modification appear imperative and must be correctly modeled to fully understand the effects. Also, the detailed shape and overall contour of the plasma-density profile may significantly affect the production of odd and

even harmonics, especially when the incident laser radiation is S polarized. Therefore, much can be learned about such plasmas from the properties of harmonic generation.

A final comment on the overall harmonic spectra is indicated. From earlier work on the nonlinearity of specularly reflected beams from clean metallic surfaces[16] it is known that large quantities of second- and third-harmonic light can be produced during reflection from turning and focusing mirrors prior to target irradiation. Dirty or contaminated surfaces can further increase these nonlinear responses. As a result, detailed studies of the lowest-order harmonic light produced in the plasma may be substantially confused by the presence of harmonic light in the beam prior to its arrival at the target.

IV. SELF-FOCUSING AND LASER FILAMENTATION

We now turn to the subject of the intensity-dependent dielectric constant and the effects of self-focusing. Equation (7) can be rewritten

$$\epsilon=1-\frac{\omega_p^2}{\omega^2}\left[1+\frac{2\alpha\lambda\!\!\!^{-}_c}{\pi c}\left[\frac{I\lambda^2}{m_0c^2}\right]\right]^{-1/2}$$

$$\approx\epsilon_0+\Delta\epsilon(I)\,, \tag{17}$$

in which $\epsilon_0=(1-\omega_p^2/\omega^2)$ represents the dielectric constant of a homogeneous plasma at low optical-field strengths. It can easily be shown that in the presence of $\Delta\epsilon(I)$ a lens is established with a focal length f, which is given by[18]

$$\frac{d}{2f}=\theta=\frac{l}{R}\sim\frac{l\Delta\epsilon}{d\epsilon_0}\,, \tag{18}$$

as seen from Fig. 11(a). Solving Eq. (18) for f we find, in the limit of $l>>f$, that

$$f=\frac{d^2}{2l}\frac{\epsilon_0}{\Delta\epsilon}\,. \tag{19}$$

The situation represented by Eq. (19) is known as the thin-lens limit. For the case where $f\sim l$, namely, the thick-lens limit, we can replace l by f in Eq. (19) arriving at the self-focusing condition[18] for a homogeneous medium,

$$f=d\left[\frac{\epsilon_0}{2\Delta\epsilon}\right]^{1/2}. \tag{20}$$

Although these relationships are approximate,

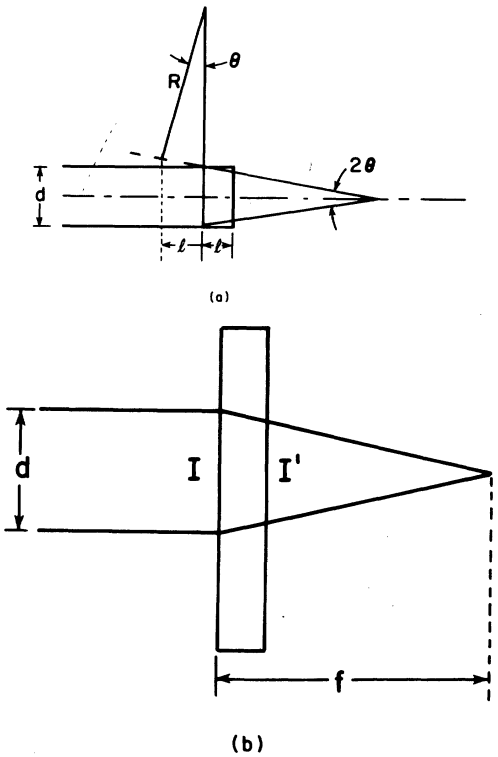

FIG. 11. Dimensioned diagrams showing the relationship of the relevant parameters connected with the self-focusing of a light beam. Part (a) shows the geometric relationship of the basic parameters whereas part (b) shows the connection between the input and output intensities in the thin-lens limit.

studies in homogeneous media have shown them to be essentially in agreement with experiments.[18,19] Figure 11(b) now shows the estimated beam intensification associated with the lens where Eq. (19) applies, namely,

$$I'=\frac{If^2}{(f-l)^2}=I\left[\frac{f/l}{f/l-1}\right]^2. \tag{21}$$

To estimate the magnitude of this effect we assume a plasma with a strongly modified density profile in the z direction similar to that calculated in Ref. 6. The laser radiation must propagate through the lower-density-shelf region assumed uniform in x and y to reach the critical density where $N_{\text{lower}}=0.1\,N_{\text{critical}}$, implying that $\omega_p^2/\omega^2=0.1$. As a specific example we assume that the lower shelf density extends over a scale length of $\sim 200\ \mu\text{m}=20\ \lambda$. This scale length corresponds to a plasma expansion velocity of $v_{\text{exp}}\sim 2\times 10^7$ cm/s over a time interval of $\sim 10^{-9}$ s. We further assume that the relevant diameter d for the beam structure is the diffraction-limited size of the focal spot associ-

ated with the $f/2.4$ focusing parabola from which a value of $d \sim 62$ μm is obtained. Typically, the measured CO_2 laser focal diameter for 80% of the energy is ~ 1.5 times this diameter. From Eqs. (17) and (20) we find that under these conditions the 10-μm beam will self-focus to a minimum diameter for an incident laser intensity of 7×10^{14} W/cm^2. Equation (17) does not include ponderomotive force effects or the spatial variation of ω_{pe} which should only enhance self-focusing. This prediction for the circumstances outlined above leads us to the view that the intensity estimated to produce 46 harmonics is produced in the target by self-focusing. In this connection, self-focusing of a CO_2 laser in a long-gradient scale-length carbon plasma has been reported.[20] Also, the observation of self-focusing in recent Nd:glass laser experiments, which used pulses of 4-ns duration,[21] provides further support because the path-integrated phase change expected in those experiments should be somewhat smaller than that expected for our present experimental conditions.

Experimentally, self-focusing appears to be strongly suggested as an explanation for the wide variation in the number of harmonics efficiently produced. Comparison of the middle spectrum of Fig. 2 with the spectrum of Fig. 6 indicates that Eq. (15) would have projected a $\sim$ threefold intensity change for constant temperature T_c. Also, in Fig. 10, the very high n_{max} at $I \sim 5 \times 10^{14}$ W/cm^2 is more easily attributable to an intensity increase of ~ 10-fold than to an unusually low $T_c \sim 5$ eV.

X-ray pinhole-camera data taken during our experiments are also consistent with self-focusing. In Fig. 12 we see four separate filtered x-ray pinhole photographs taken with ~ 1-keV photons using a pinhole doublet consisting of a 25-μm-diam pinhole and a 50-μm-diam pinhole separated by ~ 1 mm. The incident CO_2 laser intensity, as inferred from the crabeye fastest-proton detector, increases from $I \sim 4 \times 10^{14}$ W/cm^2 up to $I \sim 4 \times 10^{15}$ W/cm^2. Note how the relatively small and smooth x-ray emission region becomes broken up at the higher intensities. The emission regions in Figs.

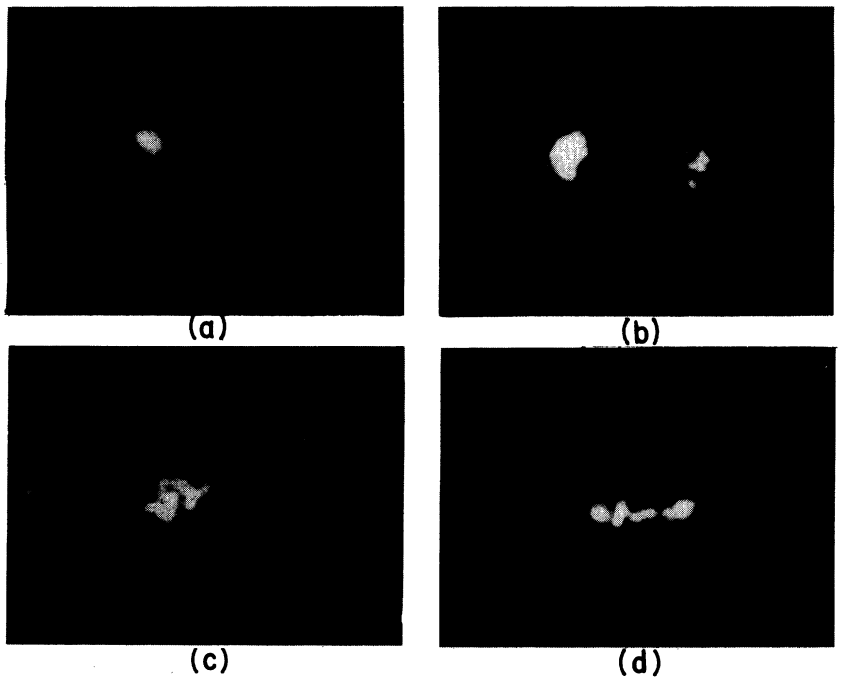

FIG. 12. X-ray pinhole-camera photographs taken simultaneously by a 25- and 50-μm-diam pinhole doublet. The two pinholes are separated by ~ 1 mm. The x-ray filtering leads to a peak sensitivity at ~ 1 keV. The four sets of photographs were taken using carbon-wire targets under otherwise identical conditions except (a) $I \sim 4 \times 10^{14}$ W/cm^2, (b) $I \sim 1.4 \times 10^{15}$ W/cm^2, (c) $I \sim 4.3 \times 10^{15}$ W/cm^2, and (d) $I \sim 2.3 \times 10^{15}$ W/cm^2. The direction of elongation is parallel to the target cylindrical axis indicating electron transport toward the target holder. The resolution-limited x-ray sources are consistent with self-focusing of the incident CO_2 radiation, but the extended size of the x-ray image along the target axis also suggests that return-current pinching could be occurring.

12(c) and 12(d) are actually resolution limited by the 25-μm-diam pinholes. On the other hand, the spatial extent of the entire emission region suggests that lateral transport and current pinching also could be occurring. Ion pinhole-camera data confirm the existence of very small emission regions in these carbon plasmas but show no similar spreading of the emission region along the axis of the wires at higher incident intensities.

An intensity-dependent dielectric constant does not affect spatial effects only; significant temporal effects can also occur.[19] Self-phase modulation will occur if the incident laser intensity varies in time (as well as due to hydrodynamics), just as self-focusing occurs if the laser intensity varies in space. As a net effect of self-phase modulation, the center frequency of the light wave in the dielectric medium is no longer a constant but becomes time dependent. The phase of the light wave ϕ is usually written

$$\phi = kz - \omega t = \frac{\sqrt{\epsilon}\omega_0}{c} z - \omega_0 t \ , \tag{22}$$

where ϵ represents the dielectric constant of the medium. The center frequency of the light wave is usually defined as the negative time derivative of this phase. When the dielectric constant ϵ is not time dependent, $-d\phi/dt = \omega_0$. However, under the present circumstances

$$-\frac{d\phi}{dt} = \omega_0 \left[1 - \frac{1}{2} \frac{z}{c} \frac{1}{\sqrt{\epsilon}} \left[\frac{d\epsilon}{dt} + v_z \frac{d\epsilon}{dz} \right] \right] , \tag{23}$$

where v_z is the velocity of the plasma along the direction of the K vector. Strictly speaking, phase accumulation should involve a spatial integration along the propagation direction where spatial self-focusing is also taken into account.[19] Although the exact solution of this problem is well beyond the scope of this paper, we wish to call attention to the spectra of Figs. 2—7. Careful analysis leads to the conclusion that the observed harmonic linewidths are ~ 100 cm^{-1} for all harmonics. The total output of the Gemini laser is contained in a bandwidth of < 0.1 cm^{-1} centered on the $P20$ transition in the 10-μm band. However, in a previous report[6] we noted the same harmonic linewidths for the Helios laser despite the fact that the output of Helios is contained typically in four transitions near $P20$ in the 10-μm band with a total spectra width of ~ 5.4 cm^{-1}. Furthermore, absolute frequency studies show that the center frequency of the nth harmonic is centered on n times the known $P20$ frequency to within 10 cm^{-1}. Numerical calculations which include these effects are required to appraise this effect.

Further suggestions that self-focusing and laser filamentation could be important come from other particle diagnostics. Directional electron beams[22] and ion beams[23] have been observed at incident CO_2 laser intensities higher than 3×10^{14} W/cm^2. In addition, very hard x rays have been seen, a fact that is consistent with a higher laser intensity than otherwise expected. On balance, the arguments presented above strongly suggest the likelihood of self-focusing.

V. CONCLUSIONS

Experimental studies of inertially confined plasmas irradiated at 10 μm with intensities $> 10^{15}$ W/cm^2 reveal the generation of strong harmonics up to the 46th order (~ 230 nm). The observed harmonics include both even- and odd-integral values as well as half-integral values. The measured efficiency of harmonic production and the polarization of the harmonic waves provide insight into the general properties of the radiating plasma oscillations. These data strongly suggest the inherent collective nature of the response.

Two aspects of the plasma response appear to be important in the production of harmonics: (1) the steep density gradient arising from the radiation pressure, and (2) self-focusing originating from an intensity-dependent correction to the index of refraction of the plasma. These data are consistent when, through the mechanism of self-focusing, the optical electric field is effectively enhanced up to tenfold. This intensification of course plays a crucial role in the generation of the high-harmonic orders observed. Using a relativistic-electron intensity-dependent correction to the normal plasma dielectric constant suggested by Kaw and Dawson[13] we find that self-focusing occurred under the prevailing experimental conditions. Further evidence also suggests the plausibility of self-focusing.

Because of the rapid response time of the electronic nonlinearity involved, we cannot rule out that four-photon parametric beating is an important process in the production of high harmonics. Numerical models are needed that can deal with

this problem in a more complete way but the space (time) resolution must be much finer than those typically used in past studies. For example, to allow harmonic orders to beat parametrically would require a time resolution of <0.1 fs to properly calculate these phenomena. Of course, a corresponding spatial resolution will also be necessary. Finally, further experiments are needed to more directly verify the presence of self-focusing during the production of these very high-harmonic orders.

ACKNOWLEDGMENTS

The authors wish to thank the operations crews of both the Helios and Gemini laser facilities for their cooperation, and D. van Hulsteyn, N. Clabo, and F. Wittman for invaluable help in taking the data. We thank D. Giovanielli, G. H. McCall, R. Godwin, D. Forslund, and J. Kindel for helpful discussions. This work was performed under the auspices of the U.S. Department of Energy.

*Permanent address: Department of Physics, University of Illinois, Chicago, Illinois 60680.

[1]For early work see, for example, N. Bloembergen and Y. R. Shen, Phys. Rev. 141, 298 (1966); A. V. Vinogradov and V. V. Pustovalov, Zh. Eksp. Teor. Fiz. 63, 940 (1972) [Sov. Phys.—JETP 36, 492 (1973)]; N. G. Basov, O. N. Krokhin, V. V. Pustovalov, A. A. Rupasov, V. P. Silin, G. V. Sklizkov, V. T. Tikhonchuk, and A. S. Shikanov, Zh. Eksp. Teor. Fiz. 67, 118 (1974) [Sov. Phys.—JETP 40, 61 (1975)]; N. S. Erokhin, S. S. Morseev, and V. V. Muklin, Nucl. Fusion 14, 333 (1974).

[2]A. Caruso, A. DeAngelis, G. Gatti, R. Gratton, and S. Martellucci, Phys. Lett. 33A, 29 (1970); M. Decroisette, B. Meyer, and Y. Vitel, *ibid.* 45A, 443 (1973); P. Lee, D. V. Giovanielli, R. P. Godwin, and G. H. McCall, Appl. Phys. Lett. 24, 406 (1974); K. Eidmann and R. Sigel, Phys. Rev. Lett. 34, 799 (1975); H. A. Baldis, H. Pepin, T. W. Johnson, and K. J. Parbhakar, *ibid.* 35, 37 (1975); A. Saleres, M. Decroisette, and C. Patou, Opt. Commun. 13, 321 (1975); A. A. Gorokhov, V. D. Dyatlov, R. N. Medvedev, A. D. Starikov, and V. G. Tuzov, Pis'ma Zh. Eksp. Teor. Fiz. 21, 111 (1975) [JETP Lett. 21, 49 (1975)]; H. A. Baldis, H. Pepin, and B. Grek, Appl. Phys. Lett. 27, 291 (1975); D. M. Phillion, R. A. Lerche, V. A. Rupert, R. A. Haas, and M. J. Boyle, Phys. Fluids 20, 1892 (1977); C. Garban, E. Farbe, C. Stenz, C. Popovics, J. Virmont, and F. Amiranoff, J. Phys. (Paris) Lett. 39, 165 (1978); H. A. Baldis, N. H. Burnett, G. D. Enright, and M. C. Richardson, Appl. Phys. Lett. 34, 327 (1979); and N. G. Basov, V. Yu. Bychenkov, O. N. Krokhin, M. V. Osipov, A. A. Rupasov, V. P. Silin, G. V. Sklizkov, A. N. Starodub, V. T. Tikhonchuk, and A. S. Shikanov, Zh. Eksp. Teor. Fiz. 76, 2094 (1979) [Sov. Phys.—JETP 49, 1059 (1979)].

[3]J. L. Bobin, M. Decroisette, B. Meyer, and Y. Vitel, Phys. Rev. Lett. 30, 594 (1973); J. L. Bobin, *Laser Interaction and Related Plasma Phenomena* (Plenum, New York, 1974), Vol. 3B, p. 591.

[4]N. H. Burnett, H. A. Baldis, M. C. Richardson, and G. D. Enright, Appl. Phys. Lett. 31, 172 (1977); and E. A. McLean, J. A. Stamper, B. H. Ripin, H. R. Griem, J. M. McMahon, and S. E. Bodner, *ibid.* 31, 825 (1977).

[5]V. V. Aleksandrov, S. I. Anisimov, M. V. Brenner, E. P. Velikhov, V. P. Vikharev, V. P. Zotov, N. G. Koval'skii, M. I. Pergament, and A. I. Yaroslavskii, Zh. Eksp. Teor. Fiz. 71, 1826 (1976) [Sov. Phys.—JETP 44, 958 (1976)]; G. Auer, K. Sauer, and K. Baumgartel, Phys. Rev. Lett. 42, 1744 (1979).

[6]R. L. Carman, D. W. Forslund, and J. M. Kindel, Phys. Rev. Lett. 46, 29 (1981).

[7]M. G. Grozeva, D. I. Metchkov, V. M. Mitev, L. I. Pavlov, and K. V. Stamenov, Opt. Commun. 23, 77 (1977).

[8]J. Reintjes, C. Y. She, and R. C. Eckardt, IEEE J. Quantum Electron. QE14, 581 (1978).

[9]V. B. Gil'denburg, Zh. Eksp. Teor. Fiz. 46, 2156 (1964) [Sov. Phys.—JETP 19, 1456 (1964)]; P. Hirsch, Radio Sci. 2, 407 (1967); Ting-Wei Tang, *ibid.* 5, 111 (1970); D. W. Forslund, J. M. Kindel, K. Lee, E. L. Lindman, and R. L. Morse, Phys. Rev. A 11, 679 (1975); J. M. Kindel, K. Lee, and E. L. Lindman, Phys. Rev. Lett. 34, 134 (1975); K. G. Estabrook, E. Valeo, and W. L. Kruer, Phys. Lett. 49A, 109 (1974); K. G. Estabrook, E. J. Valeo, and W. L. Kruer, Phys. Fluids 18, 1151 (1975); J. A. Stamper, *ibid.* 18, 735 (1975); D. W. Forslund, J. M. Kindel, K. Lee, and E. L. Lindman, Phys. Rev. Lett. 36, 35 (1976); K. Lee, D. W. Forslund, J. M. Kindel, and E. L. Lindman, Phys. Fluids 20, 51 (1977).

[10]See, for example, D. T. Attwood, D. W. Sweeney, J. M. Auerbach, and P. H. Y. Lee, Phys. Rev. Lett. 40, 184 (1978) and references cited therein.

[11]T. H. Tan, G. H. McCall, and A. H. Williams, Los Alamos Scientific Laboratory Report No. LA-UR-80-900 (unpublished).

[12]P. A. Jaanimagi, G. D. Enright, and M. C. Richardson, IEEE Trans. Plasma Sci. PS7, 166 (1979).

[13]P. Kaw and J. Dawson, Phys. Fluids 13, 472 (1970).

[14]J. D. Jackson, *Classical Electrodynamics* (Wiley, New York, 1962).

[15]See, for example, A. A. Galeev, Zh. Eksp. Teor. Fiz. 46, 1335 (1964) [Sov. Phys.—JETP 19, 904 (1964)].

[16]See, for example, F. Brown, R. E. Parks, and A. M. Sleeper, Phys. Rev. Lett. 14, 1029 (1965); S. S. Jha, Phys. Rev. 140, A2020 (1965).

[17]V. Cottles, D. Giovanielli, L. White, and A. H. Williams, Los Alamos Scientific Laboratory, Laser Fusion Progress Report No. LA-7328-PR (unpublished).

[18]See, for example, R. L. Carman and P. L. Kelley, Appl. Phys. Lett. 12, 241 (1968).

[19]The detailed study presented in J. Reintjes, R. L. Carman, and F. Shimizu, Phys. Rev. A 8, 1486 (1973) provides some insight into the kind of effects that might be seen in laser-produced plasmas.

[20]H. A. Baldis and P. B. Corkum, Phys. Rev. Lett. 45, 1260 (1980).

[21]M. J. Herbst, J. A. Stamper, R. R. Whitlock, R. H. Lehmbert, and B. H. Ripin, Phys. Rev. Lett. 46, 328 (1981).

[22]D. B. Giovanielli, J. F. Kephart, and A. H. Williams, J. Appl. Phys. 47, 2907 (1976).

[23]J. F. Kephart has seen such effects at the Gemini laser facility in Los Alamos.

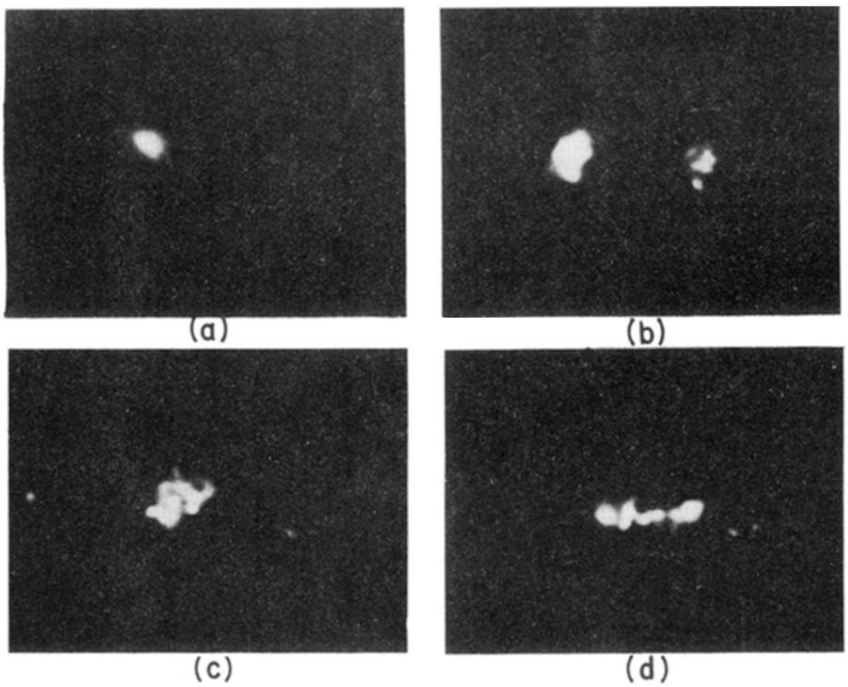

FIG. 12. X-ray pinhole-camera photographs taken simultaneously by a 25- and 50-μm-diam pinhole doublet. The two pinholes are separated by ~ 1 mm. The x-ray filtering leads to a peak sensitivity at ~ 1 keV. The four sets of photographs were taken using carbon-wire targets under otherwise identical conditions except (a) $I \sim 4 \times 10^{14}$ W/cm^2, (b) $I \sim 1.4 \times 10^{15}$ W/cm^2, (c) $I \sim 4.3 \times 10^{15}$ W/cm^2, and (d) $I \sim 2.3 \times 10^{15}$ W/cm^2. The direction of elongation is parallel to the target cylindrical axis indicating electron transport toward the target holder. The resolution-limited x-ray sources are consistent with self-focusing of the incident CO_2 radiation, but the extended size of the x-ray image along the target axis also suggests that return-current pinching could be occurring.